Long-wavelength optical phonon behavior in uniaxial strained graphene: Role of electron-phonon interaction

M. Assili and S. Haddad*

Laboratoire de Physique de la Matière Condensée, Département de Physique, Faculté des Sciences de Tunis, Université Tunis El Manar, Campus Universitaire 1060 Tunis, Tunisia

(Received 17 March 2014; revised manuscript received 15 June 2014; published 2 September 2014)

We derive the frequency shifts and the broadening of Γ-point longitudinal optical (LO) and transverse optical (TO) phonon modes, due to electron-phonon interaction, in graphene under uniaxial strain as a function of the electron density and the disorder amount. We show that, in the absence of a shear strain component, such interaction gives rise to a lifting of the degeneracy of the LO and TO modes which contributes to the splitting of the G Raman band. The anisotropy of the electronic spectrum, induced by the strain, results in a polarization dependence of the LO and TO modes. This dependence is in agreement with the experimental results showing a periodic modulation of the Raman intensity of the split G peak. Moreover, the anomalous behavior of the frequency shift reported in undeformed graphene is found to be robust under strain.

DOI: 10.1103/PhysRevB.90.125401 PACS number(s): 73.22.Pr, 63.22.Rc, 78.67.Wj, 81.05.ue

I. INTRODUCTION

Since its discovery in 2004 [1], graphene continues to be the subject of intense interest regarding its exotic properties [2,3]. These intriguing properties, such as the anomalous quantum Hall effect, are ascribed to Dirac-type electrons described by the Weyl's equation for massless particles [3]. The electronic properties in graphene are significantly affected by applying a strain [4]. The latter can also, accidentally, occur during the fabrication process as in exfoliation or chemical vapor deposition of graphene samples [5]. Theoretical and first-principles calculations revealed the substantial effect of the strain on the electronic and lattice spectra of graphene [6–9].

To bring out the signature of strain-induced modified electronic and vibrational properties, Raman spectroscopy has emerged as a powerful probe. This technique, which is simple to use in graphene, is found to be a successful tool to identify the number of layers in multilayer graphene, and to probe the nature of disorder and the doping amount [10–12].

Several experimental studies have been carried out on Raman spectra of graphene under uniaxial strain [13–22]. The results revealed that, due to the strain, the Raman G band is red-shifted and split into two peaks denoted G^+ and G^-. G^+ (G^-) is the mode-polarized perpendicular (along) the strain direction. The G peak appearing in unstrained graphene at 1580 cm^{-1} corresponds to a doubly degenerate optical mode at the Γ point of the Brillouin zone (BZ). The splitting of the G peak results from the strain-induced lattice symmetry lowering.

Experimental results showed that the frequency shift rates of the G^+ and G^- as a function of the strain strength ϵ is of $\frac{\partial\omega_{G^-}}{\partial\epsilon} \sim -13$ $cm^{-1}/\%$ and $\frac{\partial\omega_{G^+}}{\partial\epsilon} \sim -6$ $cm^{-1}/\%$ [15]. Recent measurements [17,20,22–24] reported that the rate shifts of G^- and G^+ are, respectively, of -33 and -14 $cm^{-1}/\%$ in agreement with first-principles calculations [17,23]. The difference in the shift rates was attributed to strain calibration [23]. The G-band splitting could be understood within a phenomenological model based on a semiclassical approach [17,25,26]. Within this model, the shear component of the strain is found to be responsible of the splitting.

Raman spectroscopy of strained graphene has also revealed that the 2D band, originating from a resonant scattering process involving two optical phonons at the BZ edges, splits into two peaks under uniaxial strain [23,24,27]. This splitting was ascribed to strain-induced changes in the resonant conditions resulting from both modified electronic band structure and phonon dispersion [23,25].

Several studies reported that the electron-phonon coupling plays a key role in Raman spectroscopy in graphene [2,28–30]. Ando [31] showed that, in undeformed graphene, the frequency of the center zone optical phonon mode is shifted due to electron-phonon interaction. The frequency behavior is found to depend on the value of the Fermi energy E_F compared to the phonon frequency ω_0 at the Γ point: For $E_F < \frac{\hbar\omega_0}{2}$ ($E_F > \frac{\hbar\omega_0}{2}$), the phonon frequency is red-shifted (blue-shifted) leading to a lattice softening (hardening). In the clean limit, a logarithmic singularity takes place at $E_F = \frac{\hbar\omega_0}{2}$ which is found to be smeared out in the dirty limit and at finite temperature [32]. Moreover, Ando [31] reported an anomalous behavior of the optical phonon damping induced by the electron-phonon interaction: for $E_F < \frac{\hbar\omega_0}{2}$, the phonons are damped due to the formation of electron-hole pairs leading to phonon softening [2]. However, for $E_F > \frac{\hbar\omega_0}{2}$, the phonon is no more damped since the electron-hole pair production is forbidden by the Pauli principle [2,31]. This damping behavior predicted by Ando [31] was observed in Raman spectroscopy [2,30,33].

The natural question, which arises at this point, is how the frequency shifts and damping of optical phonon are modified in uniaxial strained graphene where electron band structure is deeply changed.

Theoretical studies [34,35] showed that the perfect honeycomb lattice of graphene undergoes a quinoid-type deformation by applying a uniaxial strain. The Dirac cones are no longer at the corners of the BZ and are tilted. The corresponding low-energy electronic properties could be described by the generalized two-dimensional (2D) Weyl's Hamiltonian [35]. It

*Corresponding author: sonia.haddad@fst.rnu.tn

is worth to note that the tilted Dirac cones are also expected in the organic conductor α-(BEDT)$_2$ I$_3$ where BEDT stands for bis(ethylenedithio)-tetrathiafulvalene [35–38]. Based on the generalized Weyl's Hamiltonian, several intriguing properties of this compound have been unveiled [35,36,38,39].

In this paper, we focus on the effect of the electron-phonon interaction on the Γ-point optical phonon modes in graphene under uniaxial strain described by a quinoid-type lattice. We show that the frequency shift and the broadening of the longitudinal optical (LO) and the transverse optical (TO) phonon modes are substantially dependent on the characteristic parameters of the Weyl Hamiltonian which are the tilt and the anisotropy of the electronic dispersion relation. We bring out original points which, to the best of our knowledge, have not been addressed so far: (i) the electron-phonon interaction in strained graphene induces a lifting of the degeneracy of the LO and TO modes which contributes to the splitting of the G band. This effect is found to originate from the anisotropy of the electronic spectrum and not from the tilt of Dirac cones. The latter may only give rise to a global shift of the G band compared to the undeformed case. The splitting is found to be strongly dependent on the electron density and disorder amount. (ii) The anomalous behavior of the phonon damping reported in Refs. [2,31] in undeformed graphene is found to be a robust feature which is kept under uniaxial strain. The damping of LO and TO modes strongly depends on the strain amplitude and the phonon angle. We found that, in the particular case, where one of the modes is along the strain direction, the corresponding phonons are strongly damped for a compressive deformation. However, the phonon mode perpendicular to the strain direction is less damped and its lifetime increases as the strain amplitude increases. For tensile deformation, the mode behaviors are exchanged. (iii) A crossing of TO and LO frequencies can take place at a particular doping value as found in carbon nanotubes [40]. (iv) We found that the electron-phonon interaction contributes to the polarization dependence of the G peak in uniaxial strained graphene as concluded by Mohiuddin *et al.* [17].

The paper is organized as follows: In Sec. II, we give the outlines of the formulation to derive the optical phonon self-energy. We start with the generalized Weyl's Hamiltonian obtained within the effective mass approach. Then, we derive the electron-phonon interaction Hamiltonian and the phonon self-energy. The results are discussed in Sec. III in relation with experiments. Section IV is devoted to the concluding remarks.

II. OPTICAL PHONON SELF-ENERGY

We consider the optical phonon modes of the center BZ responsable of the G peak in graphene. We focus on the LO and in-plane TO modes. We first derive the electronic Hamiltonian, within the effective mass theory [41–43], taking into account the first- and second-neighbor hopping parameters in strained graphene.

A. Electronic Hamiltonian

By applying a uniaxial strain along, for example, the y direction, the honeycomb lattice turns to a quinoid-type lattice [3]. It is worth to note that one should consider an arbitrary strain direction as done, for example, in Refs. [6,34]. However, several experimental and numerical studies [6,17] have shown that the G-band behavior is independent of the strain direction. Considering a generic strain direction will give rise to the same form of the electronic Hamiltonian but with renormalized parameters. We then consider for simplicity a strain along the y direction as in Ref. [3]. In such case, the hopping parameters to the first-neighboring atoms are no more equal as in undeformed graphene. The distance between neighboring atoms along the y direction changes from a to

$$a' = a + \delta a.$$

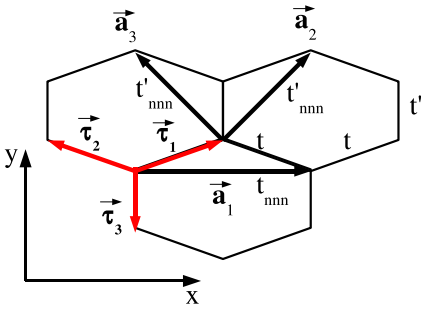

FIG. 1. (Color online) Deformed honeycomb lattice along the y axis. ($\vec{a}_1$,$\vec{a}_2$) is the lattice basis. The hopping parameters to the first (second) neighbors t and t' (t_{nnn} and t'_{nnn}) are different due the deformation. Vectors connecting first- (second-) neighboring atoms are denoted $\vec{\tau}_l$ ($\vec{a}_l$).

The vectors $\vec{\tau}_l$ ($l = 1,2,3$) connecting the sites of the A sublattice with first-neighbor sites on the B sublattice are given by (Fig. 1)

$$\vec{\tau}_1 = \frac{a}{2}(\sqrt{3}\vec{e}_x + \vec{e}_y), \quad \vec{\tau}_2 = \frac{a}{2}(-\sqrt{3}\vec{e}_x + \vec{e}_y),$$
$$\vec{\tau}_3 = -a(1+\epsilon)\vec{e}_y, \tag{1}$$

where a is the distance between first-neighbor atoms in undeformed graphene, $\epsilon = \frac{\delta a}{a}$ is the lattice deformation which measures the strain amplitude. ϵ is negative (positive) for compressive (tensile) deformation.

The second-neighbor sites are connected by vectors $\vec{a}_l$ given by

$$\vec{a}_1 = \sqrt{3}a\vec{e}_x, \quad \vec{a}_2 = \frac{\sqrt{3}}{2}a\vec{e}_x + a\left(\frac{3}{2}+\epsilon\right)\vec{e}_y,$$
$$\vec{a}_3 = -\frac{\sqrt{3}}{2}a\vec{e}_x + a\left(\frac{3}{2}+\epsilon\right)\vec{e}_y, \tag{2}$$

where ($\vec{a}_1$,$\vec{a}_2$) is the lattice basis.

The hopping integral along $\vec{\tau}_3$ is affected by the strain and is different from those along $\vec{\tau}_1$ and $\vec{\tau}_2$ which are equal. Moreover, the hopping parameters to the second-neighboring atoms along $\vec{a}_2$ and $\vec{a}_3$ are modified by the strain compared to that along $\vec{a}_1$.

It is worth to stress that by applying a strain along the y direction, one should expect a strain component along the x axis $\epsilon_{xx} = -\nu\epsilon_{yy}$ where $\nu = 0.165$ is the Poisson ratio of graphene. The off-diagonal terms of the strain tensor, which depend on the strain direction and the Poisson ratio [34], generate different bond lengths. However, for a strain axis parallel to the principal symmetry direction x or y, these terms

vanish leading to equal bond lengths as assumed in our model. The contribution of Poisson ratio could, then, be neglected compared to the main contribution resulting from the strain component along the stress axis.

We denote by $t_{nn}^{(l)}$ ($t_{nnn}^{(l)}$) the hopping integral to the first-(second-) neighboring atoms along $\vec{\tau}_l$ ($\vec{a}_l$) vectors. We set $t_{nn}^{(1)} = t_{nn}^{(2)} = t$. Under strain $t_{nn}^{(3)}$ changes from t to t' given by [35]

$$t' = t + \frac{\partial t}{\partial a}\delta a.$$

$t_{nnn}^{(l)}$ along $\vec{a}_2$ and $\vec{a}_3$ changes from the value of undeformed graphene, denoted t_{nnn}, to t'_{nnn} written as

$$t'_{nnn} = t_{nnn} + \frac{\partial t_{nnn}}{\partial a}\delta a.$$

The momentum vectors of Dirac points D and D' are given, respectively, by [35]

$$k_y^D = 0, \quad k_x^D = \xi\frac{2}{\sqrt{3}a}\arccos\left(-\frac{t'}{2t}\right), \tag{3}$$

where $\xi = \pm$ is the valley index. We denote hereafter

$$\theta = \arccos\left(-\frac{t'}{2t}\right). \tag{4}$$

In undeformed graphene, the Dirac points D and D' are at the corners of the BZ K and K'. Under the strain, D and D' move away from K and K' points [34,44].

The electronic wave function can be written as [31,43]

$$\psi(\vec{r}) = \sum_{\vec{R}_A}\psi_A(\vec{R}_A)\varphi(\vec{r}-\vec{R}_A) + \sum_{\vec{R}_B}\psi_B(\vec{R}_B)\varphi(\vec{r}-\vec{R}_B), \tag{5}$$

where $\varphi(\vec{r}-\vec{R}_A)$ and $\varphi(\vec{r}-\vec{R}_B)$ are atomic orbitals centered on atoms A and B, respectively.

In the $\vec{k}.\vec{p}$ approach [42,43], the coefficients $\psi_A(\vec{R}_A)$ and $\psi_B(\vec{R}_B)$ are given by

$$\begin{aligned}\psi_A(\vec{R}_A) &= e^{i\vec{k}^D\cdot\vec{R}_A}F_A^D(\vec{R}_A) + e^{i\vec{k}^{D'}\cdot\vec{R}_A}F_A^{D'}(\vec{R}_A),\\ \psi_B(\vec{R}_B) &= e^{i\vec{k}^D\cdot\vec{R}_B}F_B^D(\vec{R}_B) - e^{i\vec{k}^{D'}\cdot\vec{R}_B}F_B^{D'}(\vec{R}_B),\end{aligned} \tag{6}$$

where F_A^D, $F_A^{D'}$, F_B^D, and $F_B^{D'}$ are slowly varying envelope functions.

Considering second-neighbor hopping integrals, the electronic energy obeys to

$$\begin{aligned}\varepsilon\psi_A(\vec{R}_A) &= -\sum_{l=1}^{3}t_{nn}^{(l)}\psi_B(\vec{R}_A-\vec{\tau}_l) - \sum_{l=1}^{6}t_{nnn}^{(l)}\psi_A(\vec{R}_A-\vec{a}_l),\\ \varepsilon\psi_B(\vec{R}_B) &= -\sum_{l=1}^{3}t_{nn}^{(l)}\psi_A(\vec{R}_B+\vec{\tau}_l) - \sum_{l=1}^{6}t_{nnn}^{(l)}\psi_B(\vec{R}_B-\vec{a}_l),\end{aligned} \tag{7}$$

where $\vec{a}_4 = -\vec{a}_1$, $\vec{a}_5 = -\vec{a}_2$, and $\vec{a}_6 = -\vec{a}_3$.

Within the $\vec{k}.\vec{p}$ method, Eq. (7) becomes

$$\varepsilon\begin{pmatrix}F_A^D(\vec{r})\\ F_B^D(\vec{r})\end{pmatrix} = \begin{pmatrix}w_{0x}k_x & w_xk_x - iw_yk_y\\ w_xk_x + iw_yk_y & w_{0x}k_x\end{pmatrix}\begin{pmatrix}F_A^D(\vec{r})\\ F_B^D(\vec{r})\end{pmatrix}, \tag{8}$$

where $\vec{k} = (k_x,k_y)$ is the wave vector and

$$\begin{aligned}w_x &= \sqrt{3}at\sin\theta,\ w_y = \tfrac{3}{2}t'a\left(1+\tfrac{2}{3}\epsilon\right),\\ w_{0x} &= 2\sqrt{3}a(t_{nnn}\sin 2\theta + t'_{nnn}\sin\theta).\end{aligned} \tag{9}$$

Details of the calculations are given in Appendix A.

From Eq. (7) we recover the so-called minimal form of the generalized Weyl Hamiltonian [3,37]

$$H_\xi(\vec{k}) = \xi(\vec{w}_0.\vec{k}\sigma^0 + w_xk_x\sigma^x) + w_yk_y\sigma^y, \tag{10}$$

where $\vec{w}_0 = (w_{0x},w_{0y}=0)$, $\sigma^0 = 11$, σ^x and σ^y are the 2×2 Pauli matrices. The corresponding dispersion relation is of the form

$$\varepsilon_\lambda(\vec{k}) = \vec{w}_0\cdot\vec{k} + \lambda\sqrt{w_x^2k_x^2 + w_y^2k_y^2}. \tag{11}$$

$\vec{w}_0$ is responsible of the tilt of Dirac cones away from the z axis. This term obeys the condition [35]

$$\tilde{w}_0 = \sqrt{\left(\frac{w_{0x}}{w_x}\right)^2 + \left(\frac{w_{0y}}{w_y}\right)^2} < 1, \tag{12}$$

which ensures the presence of two energy bands: a positive energy for $\lambda = +$ and a negative energy band for $\lambda = -$ [35]. In deformed graphene and for $w_{0y} = 0$, $\tilde{w}_0 \sim 0.6\epsilon$ [35].

The eigenfunctions of the Hamiltonian given by Eq. (10) are of the form

$$F(\vec{k},\vec{r}) = \frac{1}{\sqrt{2S'}}\begin{pmatrix}1\\ \eta e^{i\Phi_{\vec{k}}}\end{pmatrix}e^{i\vec{k}\cdot\vec{r}}, \tag{13}$$

where $\eta = \lambda\xi$ is the chirality index, S' is the lattice surface under strain, and $\tan\Phi_{\vec{k}} = \frac{w_yk_y}{w_xk_x}$.

B. Electron-phonon interaction

In this section, we derive the effective Hamiltonian describing the effect of the lattice vibrations on the electronic Hamiltonian. Such effect arises from the change of the hopping integrals due to the lattice distortion. This Hamiltonian was obtained by Ando [31] in the case of undeformed graphene. We shall determine the electron-phonon interaction Hamiltonian in quinoid-type deformed graphene.

The phonon Hamiltonian can be written as [31]

$$H_{ph} = \sum_{\vec{q},\mu}\hbar\omega_{0,\mu}\left(b_{\vec{q},\mu}^\dagger b_{\vec{q},\mu} + \frac{1}{2}\right), \tag{14}$$

where $b_{\vec{q},\mu}^\dagger$ ($b_{\vec{q},\mu}$) is the creation (annihilation) operator of phonon with wave vector $\vec{q} = (q_x,q_y)$ and mode μ = LO, TO. $\omega_{0,\mu}$ is the μ mode phonon frequency at the Γ point.

The relative displacement of the two sublattices A and B in the continuum limit is

$$\vec{u}(\vec{r}) = \frac{1}{\sqrt{2}}[\vec{u}_A(\vec{r}) - \vec{u}_B(\vec{r})], \tag{15}$$

which can be written for optical phonon at Γ point as [31]

$$\vec{u}(\vec{r}) = \sqrt{\frac{\hbar}{2NM}}\sum_{\vec{q},\mu}\frac{1}{\omega_{0,\mu}}(b_{\vec{q},\mu} + b_{-\vec{q},\mu}^\dagger)\vec{e}_\mu(\vec{q})e^{i\vec{q}\cdot\vec{r}}, \tag{16}$$

where M is the mass of the carbon atom, N is the number of unit cells, and $\vec{e}_\mu(\vec{q})$ is given by

$$\vec{e}_L(\vec{q}) = i[\cos\varphi(\vec{q}), \sin\varphi(\vec{q})],$$
$$\vec{e}_T(\vec{q}) = i[-\sin\varphi(\vec{q}), \cos\varphi(\vec{q})] \quad (17)$$

with $\tan\varphi(\vec{q}) = \frac{q_y}{q_x}$. To derive the electron-phonon effective Hamiltonian, we shall determine the effect of the lattice displacement on the hopping integrals.

The hopping parameter between first-neighboring atoms located at $\vec{R}_A$ and $\vec{R}_A - \vec{\tau}_l$ is changed from $t_{nn}^{(l)}$ to [46]

$$t_{nn}^{(l)} + \frac{\partial t_{nn}^{(l)}}{\partial d_l}[|\vec{\tau}_l + \vec{u}_A(\vec{R}_A) - \vec{u}_B(\vec{R}_A - \vec{\tau}_l)| - d_l] \quad (18)$$

with $d_l = |\vec{\tau}_l|$, $d_1 = d_2 = a$, and $d_3 = a(1+\epsilon)$. The hopping integral between second-neighboring atoms changes from $t_{nnn}^{(l)}$ to

$$t_{nnn}^{(l)} + \frac{\partial t_{nnn}^{(l)}}{\partial a_l}[|\vec{a}_l + \vec{u}_A(\vec{R}_A) - \vec{u}_A(\vec{R}_A - \vec{a}_l)| - a_l]. \quad (19)$$

However, the correction to $t_{nnn}^{(l)}$ terms vanishes for Γ-point optical phonon modes ($\vec{q} = \vec{0}$).

Since the amplitude of the lattice displacement is small compared to the lattice parameter, Eq. (18) becomes

$$t_{nn}^{(l)} + \frac{\partial t_{nn}^{(l)}}{\partial d_l}\frac{\vec{\tau}_l}{d_l} \cdot [\vec{u}_A(\vec{R}_A) - \vec{u}_B(\vec{R}_A - \vec{\tau}_l)]. \quad (20)$$

In the continuum limit, $\vec{u}_A(\vec{R}_A) - \vec{u}_B(\vec{R}_A - \vec{\tau}_l) \simeq \vec{u}_A(\vec{r}) - \vec{u}_B(\vec{r}_A - \vec{\tau}_l) \sim \sqrt{2}\vec{u}(\vec{r})$.

The correction to the hopping integrals due to lattice distortion, given by Eq. (20), leads to an extra term ΔH in the electronic Hamiltonian which is written near the D point as (for details, see Appendix B)

$$\Delta H = \frac{\sqrt{2}}{ta}\frac{\partial t}{\partial a}\begin{pmatrix} 0 & w'_y u_y(\vec{r}) + i w_x u_x(\vec{r}) \\ w'_y u_y(\vec{r}) - i w_x u_x(\vec{r}) & 0 \end{pmatrix}, \quad (21)$$

where $u_x(\vec{r})$ and $u_y(\vec{r})$ are the component of the relative displacement $\vec{u}$. w'_y is of the form

$$w'_y = -a[t\cos\theta + t'(1+\epsilon)] \sim w_y - 2\epsilon t' a(1+\epsilon) \quad (22)$$

and θ obeys Eq. (4).

Given the expression of w_y and since $t' = t(1-2\epsilon)$ [35], we have $w_y = \frac{3}{2}at'(1+\frac{2}{3}\epsilon)$ and $w'_y = w_y - \Delta w_y$ with $\Delta w_y = \frac{4}{3}\epsilon w_y$.

The electron-phonon Hamiltonian can then be written as [31]

$$H_{int} = -\sqrt{\frac{\hbar}{NM}}\frac{\beta}{a^2}\sum_{\vec{q},\mu}\frac{1}{\sqrt{\omega_{0,\mu}}}V_\mu(\vec{q})e^{i\vec{q}\cdot\vec{r}}(b_{\vec{q},\mu} + b^\dagger_{-\vec{q},\mu}), \quad (23)$$

where $\beta = -\frac{d\ln t}{d\ln a} = -\frac{a}{t}\frac{\partial t}{\partial a}$, $\omega_{0\mu}$ is the frequency of the optical phonon at the Γ point in the deformed graphene for the mode μ in the absence of electron-phonon interaction.

In undeformed graphene, $\omega_{0T} = \omega_{0L} = \omega_0$. This degeneracy is expected to be lifted in the strained graphene due to the symmetry breaking. According to a phenomenological model [17,24,25], the strain tension ϵ_{ij} in graphene reduces to $\epsilon_{yy} = \epsilon$ where y is the direction of the applied strain, and $\epsilon_{xx} = -\nu\epsilon_{yy}$ along the direction transverse to the strain and ν is the Poisson ratio. The G band splits into two bands $G^\pm$ with frequencies $\omega^\pm$ shifted from the unstrained band frequency ω_0 as $\Delta\omega^\pm = \omega^\pm - \omega_0 = -\omega_0\gamma_{E_{2g}}(\epsilon_{xx} + \epsilon_{yy}) \pm \frac{1}{2}\beta_{E_{2g}}\omega_0(\epsilon_{xx} - \epsilon_{yy})$ where $\gamma_{E_{2g}}$ and $\beta_{E_{2g}}$ are, respectively, the Grüneisen parameter and the shear deformation potential. The shear component of the strain $\epsilon_s = \epsilon_{xx} - \epsilon_{yy}$ is then responsible of the G-band splitting. The question arising at this point concerns the contribution of the electron-phonon interaction to the splitting of the G band. To highlight this contribution, we did not consider the effect of the shear component which turns out to disregard the effect of the strain on the phonon dispersion. We then assume that, in the absence of electron-phonon interaction, the center zone optical phonon modes LO and TO have the same frequencies $\omega_{0T} \sim \omega_{0L} \sim \omega_0$. By switching on the interaction, this degeneracy may be lifted giving rise to two bands corresponding to the LO and TO modes which result in the G-band splitting.

The matrices $V_\mu(\vec{q})$ are given, near the D point, by

$$V_L(\vec{q}) = \sqrt{w_x w'_y}\begin{pmatrix} 0 & i\frac{\sin\varphi(\vec{q})}{\alpha'} - \alpha'\cos\varphi(\vec{q}) \\ i\frac{\sin\varphi(\vec{q})}{\alpha'} + \alpha'\cos\varphi(\vec{q}) & 0 \end{pmatrix},$$
$$V_T(\vec{q}) = \sqrt{w_x w'_y}\begin{pmatrix} 0 & i\frac{\cos\varphi(\vec{q})}{\alpha'} + \alpha'\sin\varphi(\vec{q}) \\ i\frac{\cos\varphi(\vec{q})}{\alpha'} - \alpha'\sin\varphi(\vec{q}) & 0 \end{pmatrix}, \quad (24)$$

where $\alpha' = \sqrt{w_x/w'_y}$. $V_\mu(\vec{q})$ near the D' point satisfies $V_\mu^{D'}(\vec{q}) = V_\mu^D(-\vec{q})^*$ [31]. Contrary to acoustic phonons, there is no scalar deformation potential in the interaction Hamiltonian [45] regarding the expression of the relative displacement of the long-wavelength optical phonons [Eq. (16)].

C. Optical phonon self-energy

The retarded phonon Green's function can be written as [31]

$$D_\mu(\vec{q},\omega) = \frac{2\hbar\omega_0}{(\hbar\omega + i\eta)^2 - (\hbar\omega_0)^2 - 2\hbar\omega_0\Pi_\mu(\vec{q},\omega)}. \quad (25)$$

$\Pi_\mu(\vec{q},\omega)$ is the self-energy and $\eta = \frac{\hbar}{\tau}$, τ being the scattering time. The shift $\Delta\omega = \omega - \omega_0$ of the phonon frequency is given by the real part of the Green's function pole. For small correction to ω_0, $\Delta\omega$ is given by

$$\Delta\omega = \frac{1}{\hbar}\mathrm{Re}\,\Pi_\mu(\vec{q},\omega_0). \tag{26}$$

The imaginary part of the Green's function pole gives the broadening $\Gamma_\mu \propto \frac{1}{\tau_\mu}$ of the phonon mode, τ_μ being the phonon lifetime:

$$\Gamma_\mu = -\frac{1}{\hbar}\mathrm{Im}\,\Pi_\mu(\vec{q},\omega_0). \tag{27}$$

The self-energy of the Γ-point optical phonon can be written as [31,46]

$$\Pi_\mu(\vec{q}\to\vec{0},\omega) = -g_v g_s \frac{\hbar S'}{NM\omega_0}\left(\frac{\beta}{a^2}\right)^2 \sum_{\lambda,\lambda'}\int \frac{d\vec{k}}{(2\pi)^2}|\langle\lambda',\vec{k}|V_\mu(\vec{q})|\lambda,\vec{k}\rangle|^2 \frac{f(\varepsilon_\lambda(\vec{k})) - f(\varepsilon_{\lambda'}(\vec{k}))}{\hbar\omega + \varepsilon_{\lambda'}(\vec{k}) - \varepsilon_\lambda(\vec{k}) + i\eta}, \tag{28}$$

where g_v and g_s are the valley and spin degeneracy, $f(\varepsilon)$ is the Fermi distribution function $f(\varepsilon) = \frac{1}{e^{\frac{\varepsilon-\mu_c}{kT}}+1}$, and μ_c is the chemical potential at temperature T. S' is the graphene surface under uniaxial strain $S' = N\|\vec{a}_1\times\vec{a}_2\| \simeq S(1+\frac{2}{3}\epsilon)$ where S is the undeformed graphene surface.

For long-wavelength phonon modes near the D point, the matrix elements can be written as

$$|\langle\lambda',\vec{k}|V_L(\vec{q})|\lambda,\vec{k}+\vec{q}\rangle|^2 = \frac{w_x w'_y}{2}\left[\frac{\sin^2\varphi(\vec{q})}{\alpha'^2}(1-\cos 2\Phi_{\vec{k}}) + \alpha'^2\cos^2\varphi(\vec{q})(1+\cos 2\Phi_{\vec{k}}) + \sin 2\varphi(\vec{q})\cos 2\Phi_{\vec{k}}\right],$$
$$|\langle\lambda',\vec{k}|V_T(\vec{q})|\lambda,\vec{k}+\vec{q}\rangle|^2 = \frac{w_x w'_y}{2}\left[\alpha'^2\sin^2\varphi(\vec{q})(1+\cos 2\Phi_{\vec{k}}) + \frac{\cos^2\varphi(\vec{q})}{\alpha'^2}(1-\cos 2\Phi_{\vec{k}}) - \sin 2\varphi(\vec{q})\cos 2\Phi_{\vec{k}}\right]. \tag{29}$$

According to Eq. (28), only interband processes ($\lambda' = -\lambda$) contribute the self-energy of $\vec{q} = \vec{0}$ phonon modes.

Regarding the electronic dispersion relation [Eq. (11)], the term $\hbar\omega + \varepsilon_{\lambda'}(\vec{k}) - \varepsilon_\lambda(\vec{k})$ in Eq. (28) becomes

$$\hbar\omega + 2\lambda\sqrt{w_x^2k_x^2 + w_y^2k_y^2}.$$

Setting $q_x = w_x k_x$ and $q_y = w_y k_y$, the integration over $\Phi_{\vec{k}}$ in Eq. (28) vanishes and the expression of the self-energy can be reduced to an integration over the energy:

$$\Pi_\mu(\vec{q}\to\vec{0},\omega) = -C_\mu\int_0^{\varepsilon_c}\frac{\varepsilon d\varepsilon}{2\pi v_F^{*2}}[f(-\varepsilon) - f(\varepsilon)]\left[\frac{1}{\hbar\omega + 2\varepsilon + i\eta} - \frac{1}{\hbar\omega - 2\varepsilon + i\eta}\right], \tag{30}$$

where we used the density of state in quinoid lattice $\rho(\varepsilon) = \frac{1}{2\pi v_F^{*2}}|\varepsilon|$ [35]. v_F^* is a renormalized Fermi velocity given by [35,47]

$$v_F^* = \sqrt{w_x w_y}\left(1 - \tfrac{3}{4}\tilde{w}_0^2\right). \tag{31}$$

ε_c in Eq. (30) is a cutoff energy corresponding to the limit of validity of the linear electronic dispersion given by Eq. (11) and the coefficient C_μ is given by

$$C_L = A\left[\frac{\sin^2\varphi(\vec{q})}{\alpha'^2} + \alpha'^2\cos^2\varphi(\vec{q})\right],$$
$$C_T = A\left[\alpha'^2\sin^2\varphi(\vec{q}) + \frac{\cos^2\varphi(\vec{q})}{\alpha'^2}\right], \tag{32}$$

and A is a constant written as

$$A = \frac{g_v g_s}{4}\frac{36\sqrt{3}}{\pi}\frac{w'_y}{w_y}\frac{S'}{S}\frac{\hbar}{2Ma^2\omega_0}\left(\frac{\beta}{2}\right)^2 \equiv C\frac{w'_y}{w_y}\frac{S'}{S}. \tag{33}$$

As mentioned in Ref. [31], one should substract the contribution of $\omega = 0$ modes to avoid double counting of electron contribution. The self-energy at zero temperature takes then the form

$$\Pi_L(\vec{q}\to\vec{0},\omega) = \frac{1}{\left(1-\tilde{w}_0^2\right)^{\frac{3}{2}}}\left[\frac{\sin^2\Phi}{\alpha'^2} + \alpha'^2\cos^2\Phi\right]\left[AE_F^* - \frac{1}{4}A(\hbar\omega + i\eta)\ln\left(\frac{\hbar\omega + 2E_F^* + i\eta}{\hbar\omega - 2E_F^* + i\eta}\right) + i\pi\right],$$
$$\Pi_T(\vec{q}\to\vec{0},\omega) = \frac{1}{\left(1-\tilde{w}_0^2\right)^{\frac{3}{2}}}\left[\alpha'^2\sin^2\Phi + \frac{\cos^2\Phi}{\alpha'^2}\right]\left[AE_F^* - \frac{1}{4}A(\hbar\omega + i\eta)\ln\left(\frac{\hbar\omega + 2E_F^* + i\eta}{\hbar\omega - 2E_F^* + i\eta}\right) + i\pi\right], \tag{34}$$

where we set $\Phi = \varphi(\vec{q})$ and $E_F^* = \hbar v_F^* k_F \simeq E_F(1-\frac{\epsilon}{3})$ (see Appendix A), with $E_F = v_F k_F$ being the Fermi energy in undeformed graphene. Equation (34) reduces to that obtained by Ando [31] in undeformed graphene for $\alpha' = 1$ and $\tilde{w}_0 = 0$.

III. RESULTS AND DISCUSSION

Figure 2 shows the dependence of the frequency shifts and broadening of the LO and the TO modes as a function of the Fermi energy E_F in the dirty limit for a compressive strain strength $\epsilon = -2\%$. The shifts are normalized to $C = A\frac{w_y}{w'_y}\frac{S}{S'}$ where A is given by Eq. (33). In an undoped system, the effect of electron-phonon interaction on the frequency shifts is not relevant. This effect is enhanced by introducing impurities in the system or by increasing the strain amplitude as we will show in the next section.

For clarity reasons, we will consider in the following strain strength $|\epsilon| \geqslant 10\%$. It should be noted that the critical strain for graphene is of 25%. Figure 3 shows the dependence of

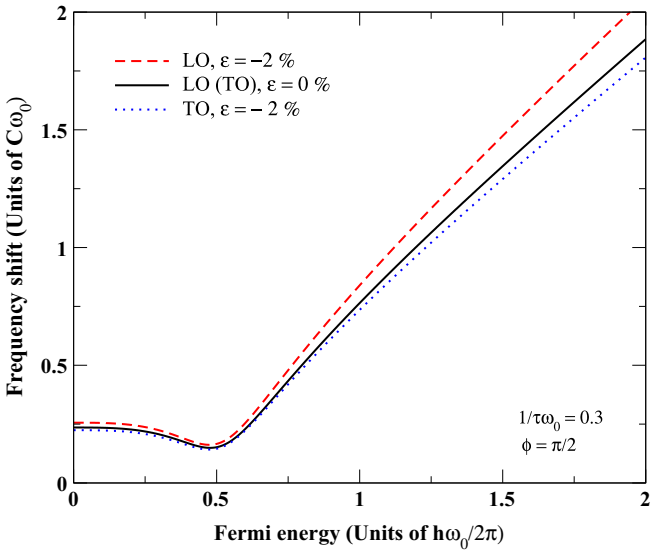

(a)

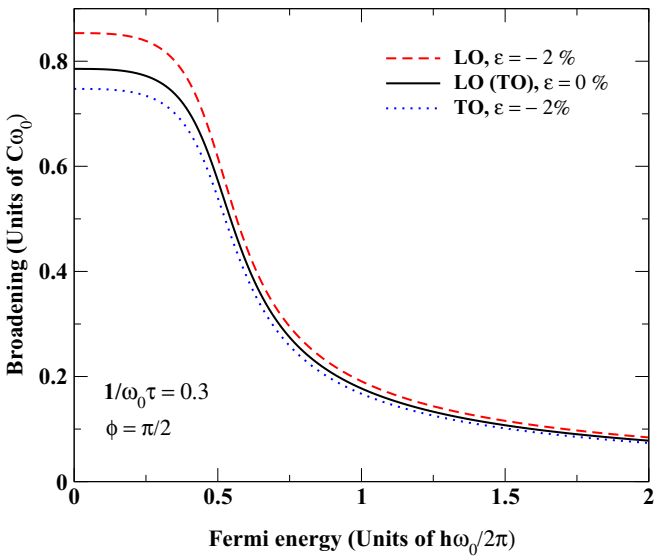

(b)

FIG. 2. (Color online) Frequency shifts (a) and broadening (b) of LO (dashed line) and TO (dotted line) modes as a function of the Fermi energy E_F in the dirty limit $\frac{1}{\tau\omega_0} = 0.3$ for a compressive strain $\epsilon = \frac{\delta a}{a} = -2\%$. The LO mode is along the strain axis. The solid line is the result for the undeformed case.

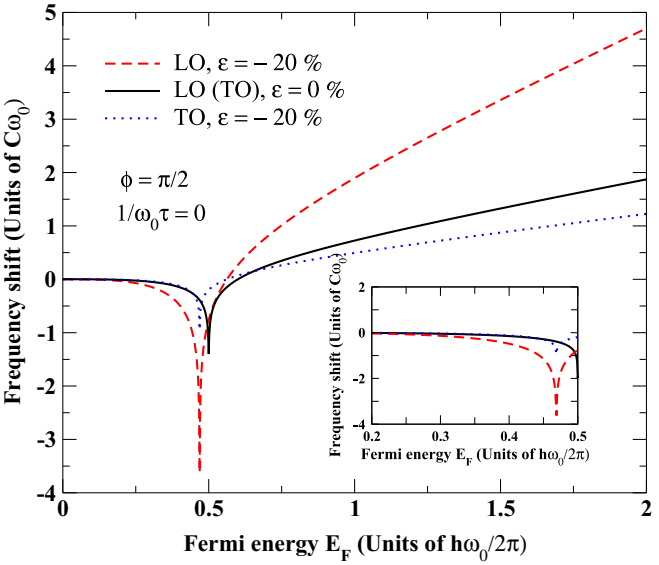

FIG. 3. (Color online) Frequency shifts of LO (dashed line) and TO (dotted line) modes as a function of the Fermi energy E_F in the clean limit ($\frac{1}{\tau\omega_0} = 0$) and for a compressive strain $\epsilon = \frac{\delta a}{a} = -20\%$. The LO mode is along the strain axis. The solid line is the result for the undeformed case. The inset shows the frequency shifts for $E_F < \frac{\hbar\omega_0}{2}$.

the frequency shifts on the Fermi energy E_F in the clean limit ($\frac{1}{\tau\omega_0} = 0$) for a compressive strain strength $\epsilon = -20\%$.

Due to the deformation, the degeneracy of LO and TO modes, obtained in the undeformed graphene (solid line in Fig. 3), is lifted. The logarithmic singularity at $E_F = \frac{\hbar\omega_0}{2}$ reported in the undeformed case is a robust feature which persists under strain but takes place at $E_F = \frac{\hbar\omega_0}{2}(1 + \frac{\epsilon}{3})$ which corresponds to $E_F^* = \frac{\hbar\omega_0}{2}$ in Eq. (34).

According to Fig. 3, both TO and LO modes are red-shifted leading to a lattice softening for $E_F < \frac{\hbar\omega_0}{2}(1 + \frac{\epsilon}{3})$. However, the phonon frequencies increase with E_F and the lattice hardens for $E_F > \frac{\hbar\omega_0}{2}(1 + \frac{\epsilon}{3})$. Moreover, the frequency of the LO mode, which is along the strain axis, is more shifted compared the the TO mode. The LO mode is then more affected by the electron-phonon interaction as shown by the broadening behavior depicted in Fig. 4. The damping of the LO mode is more pronounced than that of the TO mode which is found to be more long lived than the modes of undeformed graphene.

This behavior can be understood from the structure of the electronic dispersion. Along the strain direction, the electron velocity is enhanced for a compressive deformation ($\epsilon < 0$) as $v_y = \frac{w_y}{\hbar} \simeq \frac{3}{2\hbar}(1 - \frac{4}{3}\epsilon)at$, while that in the perpendicular direction is reduced as $v_x = \frac{w_x}{\hbar} \simeq \frac{3}{2\hbar}(1 + \frac{2}{3}\epsilon)at$.

The Fermi level changes as $E_F^* \simeq E_F(1 - \frac{\epsilon}{3})$ which increases for a compressive strain (Fig. 5). As a consequence, the production of electron-hole pairs is furthered along the strain direction, as shown in Fig. 5, since there are more states which are not blocked by Pauli principle for a given phonon frequency. However, in the direction perpendicular to the strain, electron-hole processes, allowed in the undeformed case, become forbidden by the Pauli exclusion principle. This explains the long-lived TO phonon mode compared to the modes of undeformed graphene.

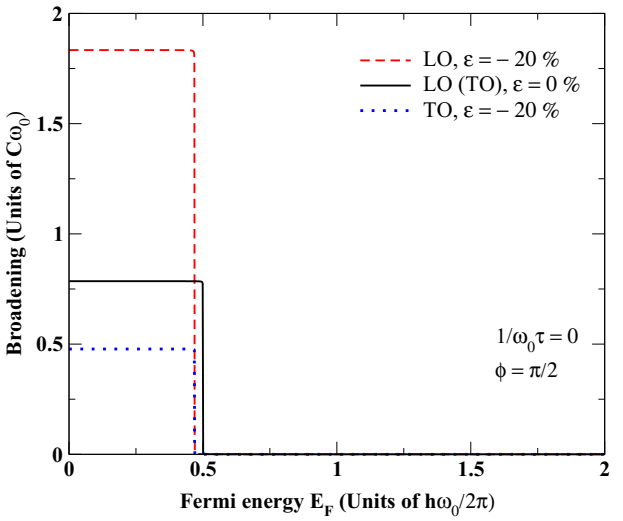

FIG. 4. (Color online) Broadenings of LO (dashed line) and TO (dotted line) modes as a function of the Fermi energy E_F in the clean limit ($\frac{1}{\tau\omega_0} = 0$) and for a compressive strain $\epsilon = \frac{\delta a}{a} = -20\%$. The LO mode is along the strain axis. The solid line is the result for the undeformed case.

The behavior of LO and TO modes is exchanged for $\Phi = 0$ where the TO mode becomes along the strain direction. Moreover, the behavior is also exchanged for tensile deformation ($\epsilon > 0$). This feature can be understood from Eq. (34) showing that the leading term for the frequency shifts is $\frac{1}{\alpha'^2} > 1$ in compressive strain and $\alpha'^2 > 1$ for tensile deformation.

Figure 6 shows the frequency shifts and the broadening of the phonon modes at $\Phi = \frac{\pi}{3}$. The difference in damping of TO and LO modes, obtained for $\Phi = \frac{\pi}{2}$ and $\Phi = 0$, is clearly reduced since both modes have a component along the strain direction.

The logarithmic singularity obtained in the clean limit at $E_F^* = \frac{\hbar\omega_0}{2}$ (Fig. 3) is smeared out in the dirty limit as shown in Fig. 7 for $\Phi = \frac{\pi}{2}$ in the case of tensile and compressive deformation. According to Fig. 7, the frequency shifts of LO and TO modes depend on the Fermi level and the amount of disorder. Away from $E_F^* \sim \frac{\hbar\omega_0}{2}$, all modes show a blue-shift contrary to the clean limit where LO and TO modes undergo a red-shift (blue-shift) for compressive (tensile) strain at $E_F^* < \frac{\hbar\omega_0}{2}$. The frequency blue-shift is reminiscent of that found by Ando [31] in undeformed graphene in the dirty limit.

The dependence of the frequency shifts on the doping level and the amount of disorder may explain the discrepancy in the experimental values of the shift rates of G^+ and G^- bands as function of the strain [15–17,20,22] and which was ascribed to a difference in the strain calibration. We suggest that this discrepancy may be due to the doping and the disorder amount in the sample.

In Ref. [22], the authors studied the behavior of the G band in deformed graphene using polarized light. They reported that the G peak can be regarded as a mixture of three peaks corresponding to the undeformed case (G^0), and compressive (G^-) and tensile (G^+) deformation. The authors attributed the presence of both blue- and red-shifted frequencies (G^+ and G^- bands) to the anisotropy of the applied deformation.

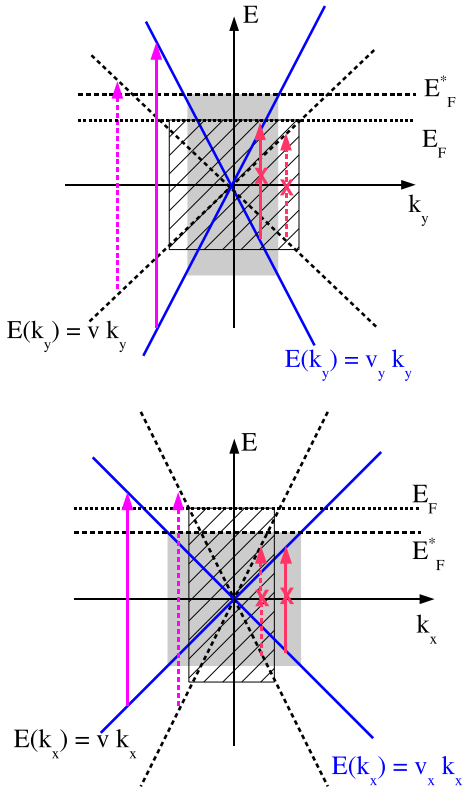

FIG. 5. (Color online) Electron-hole process responsible of phonon hardening corresponds to the states where production of electron-hole pairs is forbidden by the Pauli principle. These states correspond to the dashed region for undeformed case and the gray area for compressive strain. The Fermi level (E_F^*) increases under compressive deformation and the Fermi velocity v_y (v_x) along (perpendicular) to the strain direction ($y'y$) is enhanced (reduced) compared to the isotropic case. This leads to more (less) electron-hole pairs contributing to phonon softening. The dashed and solid arrows (crossed solid and dashed arrows) denote the electron-hole process leading to phonon softening (hardening) for the undeformed and compressed case, respectively.

According to Figs. 3 and 7, for $E_F^* > \frac{\hbar\omega_0}{2}$ and $\Phi = \frac{\pi}{2}$, the LO mode (TO mode) is blue-shifted (red-shifted) compared to the undeformed mode (solid line in the figures) for compressive strain. The experimental results of Ref. [22] could then be the signature of the electron-phonon interaction. The shifted G^+ and G^- modes could be assigned to the LO and TO modes for a given uniaxial strain at a doping level $E_F^* > \frac{\hbar\omega_0}{2}$.

In Fig. 8, we plot the broadening of phonon modes as a function of the Fermi energy for $\Phi = \frac{\pi}{2}$ in the dirty limit. The figure shows that the damping of the mode along the strain direction is enhanced as the amplitude of the deformation increases. This reflects the increasing number of the electron-hole pairs leading to decaying phonons (Fig. 5).

The strain dependence of the frequency shifts is depicted in Fig. 9 where we considered the case of undoped graphene in the dirty limit ($E_F = 0$, $\frac{1}{\tau\omega_0} = 0.1$) and the doped graphene ($\frac{E_F}{\hbar\omega_0} = 0.45$) in the clean limit since the shifts in the clean undoped case are small. The shift behaviors could be understood from the processes depicted in Fig. 5.

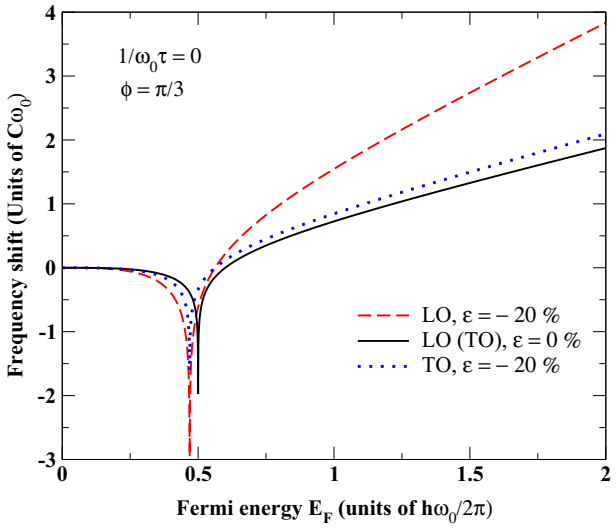

(a)

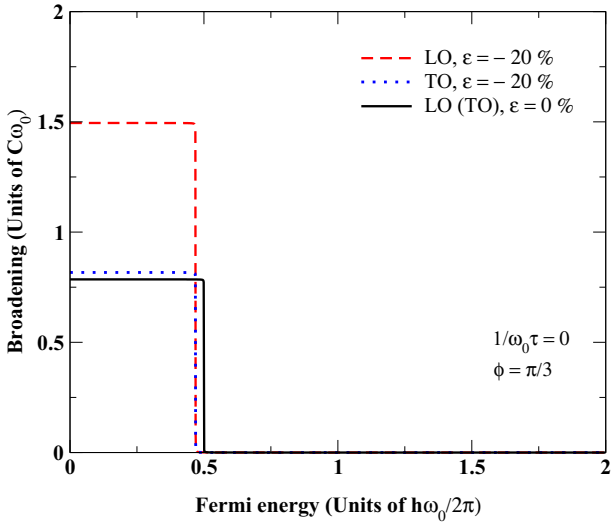

(b)

FIG. 6. (Color online) Frequency shifts and broadenings of LO (dashed line) and TO (dotted line) modes as a function of the Fermi energy E_F in the clean limit ($\frac{1}{\tau\omega_0} = 0$) and for a compressive deformation $\epsilon = \frac{\delta a}{a} = -20\%$. The phonon angle is $\Phi = \frac{\pi}{3}$. The solid line is the result for the undeformed case.

Figure 9 shows a linear behavior of the frequency shift as a function of the strain strength for small strain. This is reminiscent of the experimental results reported in Refs. [17,20]. The strain rates and slopes of the frequency shifts are dependent on the doping level and the disorder amount. According to Fig. 9, the linearity is lost by increasing the strain. It is worth to note that a departure from a linear behavior was also reported in Ref. [23] for the strain dependence of the frequency shift of the 2D Raman band. Such behavior could also be observed in Raman spectra of α-$(BEDT)_2 I_2$ salt showing a strong anisotropic electronic Dirac spectrum.

In the limit of strong strain, we expect a decoupling of electron-hole pairs from the phonon mode along (perpendicular) to the strain axis for tensile (compressive) deformation as shown in Fig. 10. Such effect could not be observed in graphene

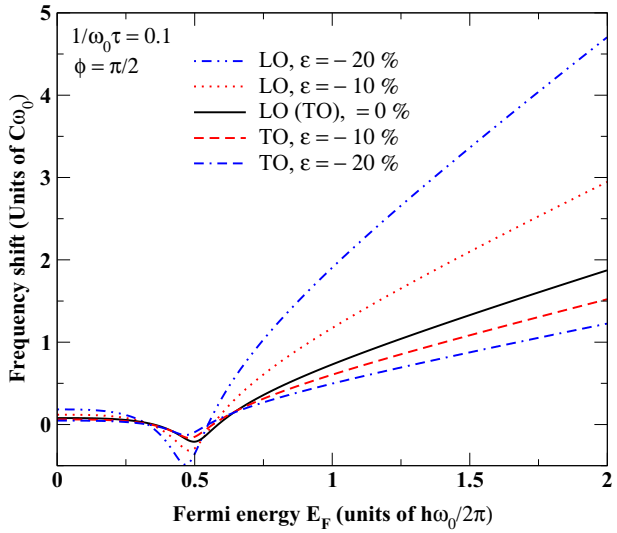

FIG. 7. (Color online) Frequency shifts of LO and TO modes as a function of the Fermi energy E_F in the dirty limit ($\frac{1}{\tau\omega_0} = 0.1$) and for compressive strains of -10% and -20%. The LO phonon mode is along the strain direction. The solid line is the result for the undeformed case.

where the critical strain is of 25% but may be brought out in α-$(BEDT)_2$ [48,49].

A hallmark feature of the doping dependence of the frequency shifts is the presence of crossings of LO and TO modes (Figs. 3 and 7). At the corresponding Fermi energy, no G-band splitting is expected due to electron-phonon interaction. Experimentally, the G^+ and the G^- bands should then merge in uniaxial strained graphene by doping the sample at the critical value corresponding to the crossing of LO and TO modes. This feature could only be observed in the absence of the shear strain which induces a splitting of the G band. A

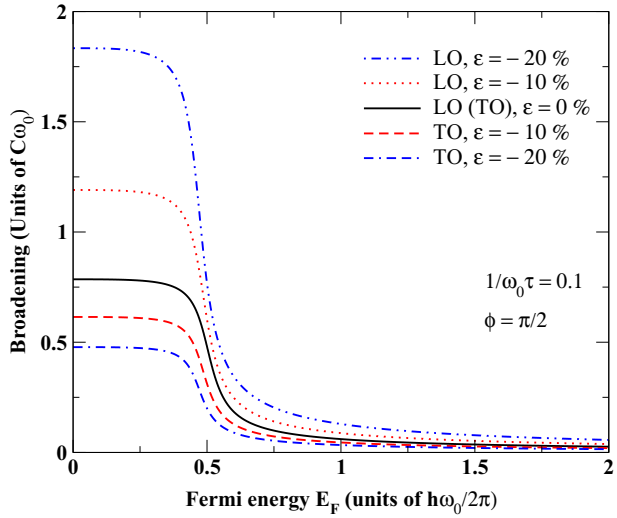

FIG. 8. (Color online) Broadenings of LO and TO modes as a function of the Fermi energy E_F in the dirty limit ($\frac{1}{\tau\omega_0} = 0.1$) and for compressive strains of -10% and -20%. The LO phonon mode is along the strain direction. The solid line is the result for the undeformed case.

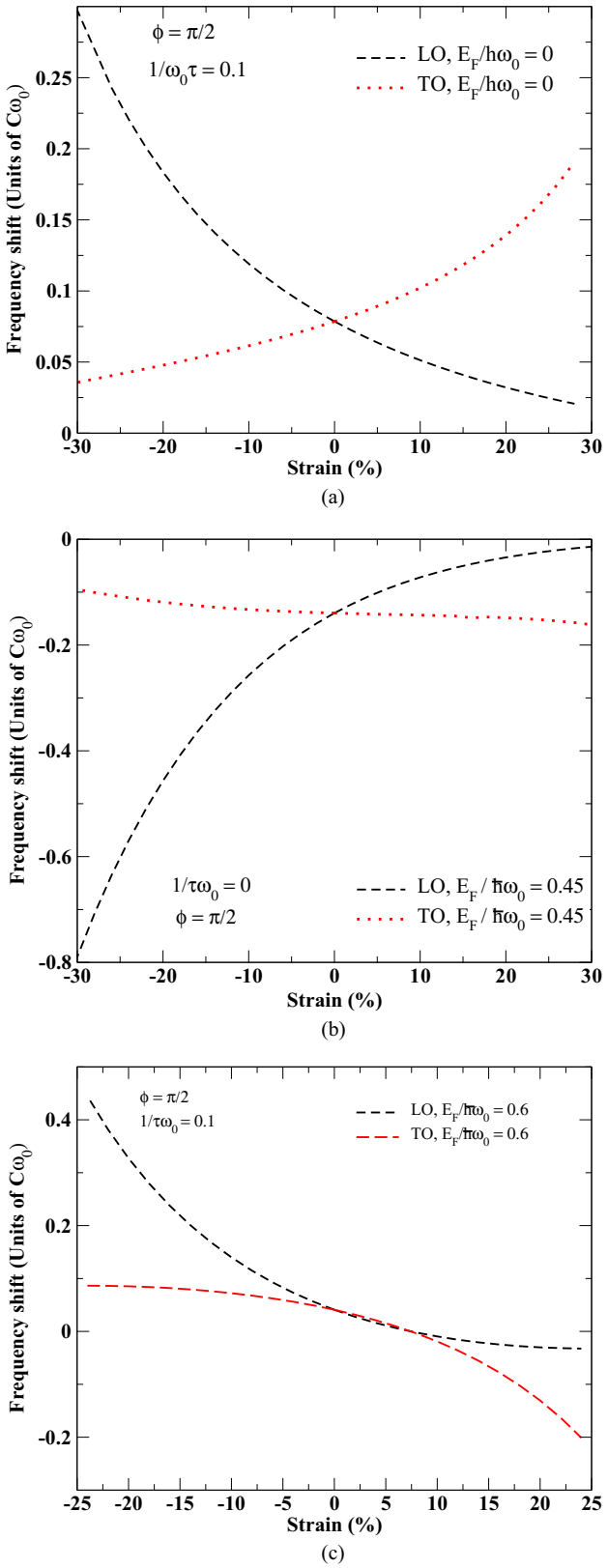

FIG. 9. (Color online) Strain dependence of the of LO (dashed line) and TO (dotted line) frequency shifts in (a) undoped case and in the dirty limit ($\frac{1}{\tau\omega_0} = 0.1$), (b) in doped case ($\frac{E_F}{\hbar\omega_0} = 0.45$) and in the clean limit ($\frac{1}{\tau\omega_0} = 0$), and (c) in doped case ($\frac{E_F}{\hbar\omega_0} = 0.6$) and in the dirty limit ($\frac{1}{\tau\omega_0} = 0.1$). The LO phonon mode is along the strain direction.

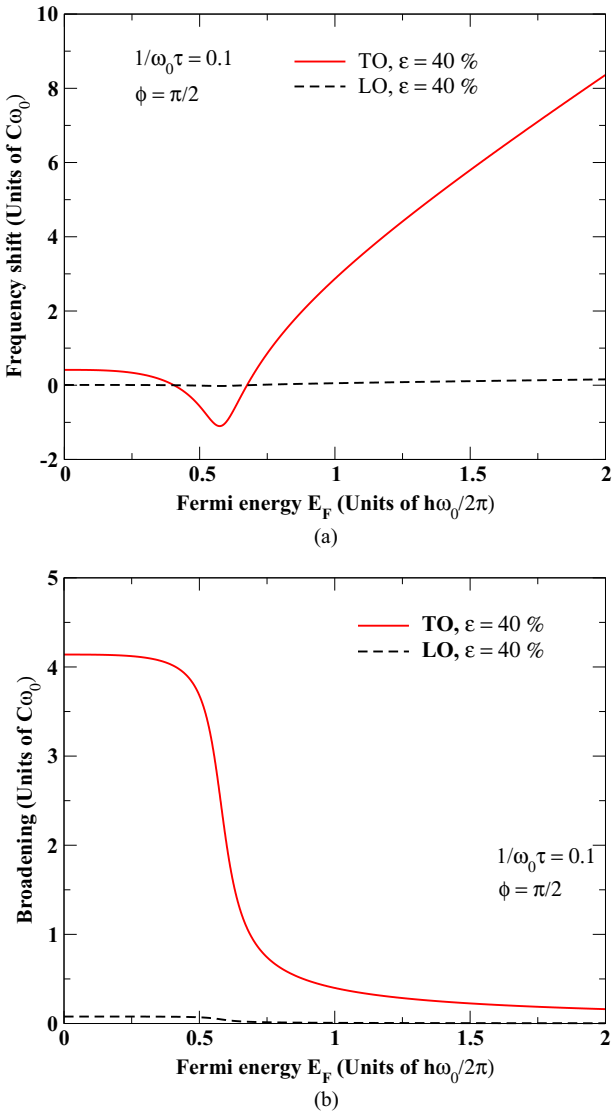

FIG. 10. (Color online) (a) Frequency shifts and (b) broadenings of the of LO (dashed line) and TO (solid line) as a function of the Fermi energy E_F in the dirty limit ($\frac{1}{\tau\omega_0} = 0.1$) and for a strong tensile deformation. The LO phonon mode, which is along the strain direction, decouples from the electron-hole pairs.

possible crossing of LO and TO modes was also reported in carbon nanotubes [40].

In Fig. 11, we plot the dependence of the phonon frequency shifts on the phonon angle Φ with respect to the axis perpendicular to the strain direction. The shifts of the LO and TO modes display a periodic modulation with a relative shift of 90°. According to Eq. (34), this dependence is due to the anisotropy of the electronic dispersion relation. Considering the isotropic case ($\alpha' = 1$), the shifts become independent on Φ as in isotropic honeycomb lattice [31].

Our results are in agreement with the experimental data [17,22] and numerical calculations [25] showing a periodic modulation of the intensity of G^+ and the G^- peaks as a function of the angle between the incident light polarization and the strain axis. The relative shifts of the two bands are also found to be of 90°. Our results support the idea presented

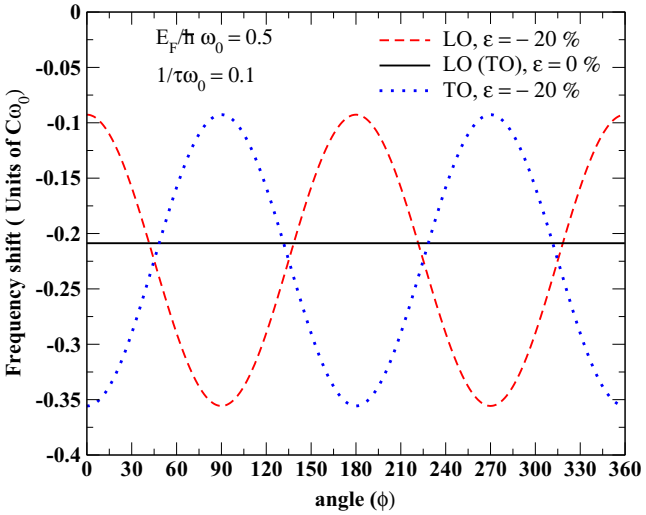

FIG. 11. (Color online) Angle dependence of the frequency shifts of the LO (dashed line) and TO (dashed-dotted line) in the doped case ($E_F = 0.5\hbar\omega_0$), in the dirty limit ($\frac{1}{\tau\omega_0} = 0.1$), and for a compressive deformation. Φ (in degrees) is the angle of optical phonon with respect to the x axis perpendicular to the strain direction. The solid line is the result for the undeformed case.

in the experimental study of Mohiuddin *et al.* [17] suggesting that the polarization dependence of the G peaks is due to the anisotropy of the electronic spectrum and such dependence is the signature of the electron-phonon interaction. It is worth to stress that Sasaki *et al.* [50] proposed that the nature of the graphene edges contributes also to the polarization dependence of Raman bands in strained graphene.

IV. CONCLUDING REMARKS

We have derived the frequency shifts and the broadenings of the longitudinal (LO) and transverse (TO) optical phonon modes at the Γ point in graphene under uniaxial strain disregarding the contribution of shear strain component. We show that the Raman G band, corresponding to a double-degenerate mode in undeformed graphene, may split into two peaks due to electron-phonon interaction. These peaks are assigned to the LO and the TO modes which are found to be strongly dependent on the Fermi level and the amount of disorder. This dependence may explain the difference in the experimental results giving the strain rates of the frequency shifts of the G^+ and G^- modes.

Moreover, we found that the splitting of the G band is due to the anisotropy of the electronic spectrum. The tilt of Dirac cones, arising also from the strain, is found to be irrelevant for the relative frequency shift of the LO and TO modes since it leads to a global shift of the G peak.

We also show that the electron-phonon intercation contributes to the Raman polarization dependence of the G peaks in strained graphene. This contribution reflects the anisotropy of the electronic spectrum. The optical phonon mode along the strain is found to be damped (long lived) for compressive (tensile) strain. The frequency shifts and the lifetime of the optical phonons are substantially dependent on the strain strength and the phonon angle. At relatively strong strain, it is possible to induce a decoupling of the phonon mode perpendicular to the compressive strain axis from electron-hole pair production process. The signature of the strain-induced anisotropic electronic dispersion could also be brought out in the Γ-point magnetophonon resonance at high magnetic field [51].

ACKNOWLEDGMENTS

We thank Y.-W. Son and K. Sasaki for helpful and stimulating discussions. We thank J.-N. Fuchs for a critical reading of the manuscript. This work was partially supported by the National Research Foundation of Korea (NRF) grant funded by the Korea government (MEST) (Grant No. 2011-0030902). S.H. acknowledges the kind hospitality of W. Kang and the members of CERC (Seoul, Korea). The final form of the manuscript was prepared in the ICTP (Trieste, Italy). S.H. was supported by Simons-ICTP associate fellowship.

APPENDIX A: WEYL HAMILTONIAN BY $\vec{k}\cdot\vec{p}$ METHOD

The $\vec{k}\cdot\vec{p}$ method was used by Ando [31,42] to derive the Dirac Hamiltonian in undeformed graphene taking only into account the hopping integral to the first-neighboring carbon atoms. Following Ref. [31], we derive the Weyl Hamiltonian for uniaxial strained graphene considering first- and second-neighboring hopping integrals. We start with the eigenproblem given by Eq. (7) where the functions $\psi_A(\vec{R}_A)$ and $\psi_B(\vec{R}_B)$ are written as

$$\psi_A(\vec{R}_A) = a^\dagger(\vec{R}_A)\Phi_A(\vec{R}_A),$$
$$\psi_B(\vec{R}_B) = b^\dagger(\vec{R}_B)\Phi_B(\vec{R}_B), \tag{A1}$$

where the vectors $a(\vec{R}_A)$, $b(\vec{R}_B)$, $\Phi_A(\vec{R}_A)$, and $\Phi_B(\vec{R}_B)$ are given by

$$a(\vec{R}_A) = \begin{pmatrix} e^{-i\vec{k}^D\cdot\vec{R}_A} \\ e^{-i\vec{k}^{D'}\cdot\vec{R}_A} \end{pmatrix}, \quad b(\vec{R}_B) = \begin{pmatrix} e^{-i\vec{k}^D\cdot\vec{R}_B} \\ -e^{-i\vec{k}^{D'}\cdot\vec{R}_B} \end{pmatrix},$$
$$\Phi_A(\vec{R}_A) = \begin{pmatrix} F_A^D(\vec{R}_A) \\ F_A^{D'}(\vec{R}_A) \end{pmatrix}, \quad \Phi_B(\vec{R}_B) = \begin{pmatrix} F_B^D(\vec{R}_B) \\ F_B^{D'}(\vec{R}_B) \end{pmatrix}. \tag{A2}$$

The left-hand side of Eq. (7) can be written, at $\vec{R}_A$, as

$$\varepsilon a^\dagger(\vec{R}_A)F_A(\vec{R}_A) = \varepsilon\sum_{\vec{R}_A} g(\vec{r}-\vec{R}_A)a(\vec{R}_A)a^\dagger(\vec{R}_A)F_A(\vec{R}_A), \tag{A3}$$

where $g(\vec{r})$ is a smoothing function satisfying

$$\sum_{\vec{R}_A} g(\vec{r}-\vec{R}_A) = \sum_{\vec{R}_B} g(\vec{r}-\vec{R}_B) = 1,$$
$$f(\vec{r})g(\vec{r}-\vec{R}_A) \simeq f(\vec{R})g(\vec{r}-\vec{R}). \tag{A4}$$

$f(\vec{r})$ is an envelope function [31]. These properties yield to

$$\sum_{\vec{R}_A} g(\vec{r}-\vec{R}_A)e^{i(\vec{k}^{D'}-\vec{k}^D)\cdot\vec{R}_A}$$
$$= \sum_{\vec{R}_B} g(\vec{r}-\vec{R}_B)e^{i(\vec{k}^{D'}-\vec{k}^D)\cdot\vec{R}_B} \simeq 0,$$
$$\sum_{\vec{R}_A} g(\vec{r}-\vec{R}_A)a(\vec{R}_A)a^\dagger(\vec{R}_A) \simeq \begin{pmatrix} 1 & 0 \\ 0 & 1 \end{pmatrix}, \tag{A5}$$

which is reminiscent of the δ function [31]. Equation (7) can then be written, around the A site, as

$$\varepsilon \sum_{\vec{R}_A} g(\vec{r}-\vec{R}_A)a(\vec{R}_A)a^\dagger(\vec{R}_A)F_A(\vec{r}) = -\sum_{l=1}^{3} t_{nn}^{(l)} \sum_{\vec{R}_A} g(\vec{r}-\vec{R}_A)a(\vec{R}_A)b^\dagger(\vec{R}_B)F_B(\vec{r}-\vec{\tau}_l) - \sum_{l=1}^{6} t_{nnn}^{(l)} \sum_{\vec{R}_A} g(\vec{r}-\vec{R}_A)a(\vec{R}_A)a^\dagger(\vec{R}_A-\vec{a}_l)F_A(\vec{r}-\vec{a}_l). \tag{A6}$$

The left-hand side of Eq. (A6) reduces to $\varepsilon F_A(\vec{R}_A)$, and in the right-hand side we set

$$F_B(\vec{r}-\vec{\tau}_l) \simeq F_B(\vec{r}) - \left(\vec{\tau}_l \cdot \frac{\partial}{\partial \vec{r}}\right) F_B(\vec{r}),$$
$$F_A(\vec{r}-\vec{a}_l) \simeq F_A(\vec{r}) - \left(\vec{a}_l \cdot \frac{\partial}{\partial \vec{r}}\right) F_A(\vec{r}). \tag{A7}$$

We then obtain

$$\sum_{\vec{R}_A} g(\vec{r}-\vec{R}_A)a(\vec{R}_A)b^\dagger(\vec{R}_A-\vec{\tau}_l) \simeq \begin{pmatrix} e^{i\vec{k}^D\cdot\vec{\tau}_l} & 0 \\ 0 & -e^{-i\vec{k}^{D'}\cdot\vec{\tau}_l} \end{pmatrix}. \tag{A8}$$

Applying this term to $F_B(\vec{r})$ in Eq. (A6) and summing over l gives rise to a diagonal term of the form $(2\cos\theta)\mathbb{1} = -\frac{t'}{t}\mathbb{1}$ which leads to a shift of the total energy.

The term $(\vec{\tau}_l \cdot \frac{\partial}{\partial \vec{r}})F_B(\vec{r})$ in Eq. (A7), summed over l and applied to $F_B(\vec{r})$, gives

$$\sum_l \left(\vec{\tau}_l \cdot \frac{\partial}{\partial \vec{r}}\right) \begin{pmatrix} F_B^D(\vec{r}) \\ F_B^{D'}(\vec{r}) \end{pmatrix} = \begin{pmatrix} t[-a\sqrt{3}\sin\theta\, k_x + ia\cos\theta\, k_y - iat'(1+\epsilon)k_y]F_B^D(\vec{r}) \\ t[a\sqrt{3}\sin\theta\, k_x + ia\cos\theta\, k_y - iat'(1+\epsilon)k_y]F_B^{D'}(\vec{r}) \end{pmatrix}. \tag{A9}$$

In Eq. (A6), the contribution of the first-neighbor hopping integrals gives then rise to the following eigenproblem near the D point:

$$\varepsilon F_A(\vec{r}) = \begin{pmatrix} w_x k_x - i w_y k_y & 0 \\ 0 & w_x k_x + i w_y k_y \end{pmatrix} F_B(\vec{r}), \tag{A10}$$

where $w_x = \sqrt{3}at\sin\theta$, $w_y = -ta\cos\theta + t'a(1+\epsilon) = \frac{3}{2}t'(1+\frac{2}{3}\epsilon)a$, $k_x = -i\frac{\partial}{\partial x}$, and $k_y = -i\frac{\partial}{\partial y}$.

For the second-neighbor hopping integrals, one has

$$\sum_{\vec{R}_A} g(\vec{r}-\vec{R}_A)a(\vec{R}_A)a^\dagger(\vec{R}_A-\vec{a}_l) \simeq \begin{pmatrix} e^{i\vec{k}^D\cdot\vec{a}_l} & 0 \\ 0 & e^{-i\vec{k}^{D'}\cdot\vec{a}_l} \end{pmatrix} \tag{A11}$$

and

$$\sum_l t_{nnn}^{(l)} e^{-i\vec{k}^D\cdot\vec{a}_l}\left(\vec{a}_l \cdot \frac{\partial}{\partial \vec{r}}\right) = w_{0x}k_x, \tag{A12}$$

where $w_{0x} = 2\sqrt{3}a(t_{nnn}\sin 2\theta + t'_{nnn}\sin\theta)$.

The electronic Hamiltonian, near the D and D' points, takes the form

$$H_\xi^D = \xi \begin{pmatrix} w_{0x}k_x & w_x k_x - i\xi w_y k_y \\ w_x k_x + i\xi w_y k_y & w_{0x}k_x \end{pmatrix} \tag{A13}$$

with $\xi = +(-)$ at the $D\,(D')$ point.

w_x and w_y can be expressed as a function of the strain strength as

$$w_x = \sqrt{3}at\sin\theta \simeq \tfrac{3}{2}at\left(1+\tfrac{2}{3}\epsilon\right), \tag{A14}$$

$$w_y = \tfrac{3}{2}t'\left(1+\tfrac{2}{3}\epsilon\right)a \simeq \tfrac{3}{2}at\left(1-\tfrac{4}{3}\epsilon\right). \tag{A15}$$

In graphene, $\tilde{w}_0 = \sqrt{(\frac{w_{0x}}{w_x})^2 + (\frac{w_{0y}}{w_y})^2} \simeq 0.6\epsilon$ [35]. In the present case, we have $w_{0y} = 0$.

APPENDIX B: ELECTRON-PHONON EFFECTIVE HAMILTONIAN

Regarding the effect of the lattice distortion on the hopping integral [Eq. (18)], an extra term appears in the electronic Hamiltonian [Eq. (A13)]. This term arises from the contribution of the hopping-term correction $\frac{\partial t_{nn}^{(l)}}{\partial d_l}$ in Eq. (7). This contribution is of the form

$$\sum_l \sum_{\vec{R}_A} g(\vec{r}-\vec{R}_A)a(\vec{R}_A)b(\vec{R}_A-\vec{\tau}_l)\left(-\frac{\partial t_{nn}^{(l)}}{\partial d_l}\right)\sqrt{2}\left(\frac{\vec{\tau}_l}{d_l}\right)\cdot\vec{u}(\vec{r})F_B(\vec{r}) = \sum_l \begin{pmatrix} e^{-i\vec{k}^D\cdot\vec{\tau}_l} & 0 \\ 0 & -e^{-i\vec{k}^{D'}\cdot\vec{\tau}_l} \end{pmatrix}\left(-\frac{\partial t_{nn}^{(l)}}{\partial d_l}\right)\sqrt{2}\left(\frac{\vec{\tau}_l}{d_l}\right)\cdot\vec{u}(\vec{r})F_B(\vec{r}), \tag{B1}$$

where the summation over l around the D point gives

$$\sum_l -e^{-i\vec{k}^D\cdot\vec{\tau}_l}\left(-\frac{\partial t_{nn}^{(l)}}{\partial d_l}\right)\sqrt{2}\left(\frac{\vec{\tau}_l}{d_l}\right)\cdot\vec{u}(\vec{r}) = \frac{\sqrt{2}}{ta}\left(\frac{\partial t}{\partial a}\right)[iw_x u_x + w'_y u_y], \tag{B2}$$

where $d_l = a$ and we used the Harrison's law [35]: $\frac{1}{t_{nn}d_l}(\frac{\partial t_{nn}^{(l)}}{\partial d_l}) = -\frac{2}{d_l^2}$. Here, $w'_y = w_y - 2\epsilon t'a(1+\epsilon) \simeq w_y(1-\frac{4}{3}\epsilon)$. This contribution gives rise to the effective phonon-electron Hamiltonian given by Eq. (21).

[1] K. S. Novoselov, A. K. Geim, S. V. Morozov, D. Jiang, Y. Zhang, S. V. Dubonos, I. V. Grigorieva, and A. A. Firsov, Science **306**, 666 (2004); K. S. Novoselov, A. K. Geim, S. V. Morozov, D. Jiang, M. I. Katsnelson, I. V. Gregorieva, S. V. Dubonos, and A. A. Firsov, Nature (London) **438**, 197 (2005).

[2] A. H. Castro Neto, F. Guinea, N. M. R. Peres, K. S. Novoselov, and A. K. Geim, Rev. Mod. Phys. **81**, 109 (2009).

[3] M. Goerbig, Rev. Mod. Phys. **83**, 1193 (2011).

[4] F. M. D. Pellegrino, G. G. N. Angilella, and R. Pucci, Phys. Rev. B **81**, 035411 (2010).

[5] N. M. R. Peres, Rev. Mod. Phys. **82**, 2673 (2010).

[6] M. Mohr, K. Papagelis, J. Maultzsch, and C. Thomsen, Phys. Rev. B **80**, 205410 (2009).

[7] Y. C. Cheng, Z. Y. Zhu, G. S. Huang, and U. Schwingenschlogl, Phys. Rev. B **83**, 115449 (2011).

[8] M. Vozmediano, M. Katsnelson, and F. Guinea, Phys. Rep. **496**, 109 (2010).

[9] F. de Juan, M. Sturla, and M. A. H. Vozmediano, Phys. Rev. Lett. **108**, 227205 (2012).

[10] L. M. Malard, M. A. Pimenta, G. Dresselhaus, and M. S. Dresselhaus, Phys. Rep. **473**, 51 (2009).

[11] A. Jorio, M. S. Dresselhaus, R. Saito, and G. Dresselhaus, *Raman Spectroscopy in Graphene Related Systems* (Wiley, Hoboken, NJ, 2011).

[12] A. C. Ferrari and D. Basko, Nat. Nanotechnol. **8**, 235 (2013).

[13] N. Ferralis, R. Maboudian, and C. Carraro, Phys. Rev. Lett. **101**, 156801 (2008).

[14] Z. H. Ni, W. Chen, X. F. Fan, J. L. Kuo, T. Yu, A. T. S. Wee, and Z. X. Shen, Phys. Rev. B **77**, 115416 (2008).

[15] M. Huang, H. Yan, C. Chen, D. Song, T. F. Heinz, and J. Hone, Proc. Natl. Acad. Sci. USA **106**, 7304 (2009).

[16] Z. H. Ni, T. Yu, Y. H. Lu, Y. Y. Wang, Y. P. Feng, and Z. X. Shen, ACS Nano **2**, 2301 (2008).

[17] T. M. G. Mohiuddin, A. Lombardo, R. R. Nair, A. Bonetti, G. Savini, R. Jalil, N. Bonini, D. M. Basko, C. Galiotis, N. Marzari, K. S. Novoselov, A. K. Geim, and A. C. Ferrari, Phys. Rev. B **79**, 205433 (2009).

[18] O. Frank, G. Tsoukleri, J. Parthenios, K. Papagelis, I. Riaz, R. Jalil, K. S. Novoselov, and C. Galiotis, ACS Nano **4**, 3131 (2010).

[19] O. Frank, G. Tsoukleri, I. Riaz, K. Papagelis, J. Parthenios, A. C. Ferrari, A. K. Geim, K. S. Novoselov, and C. Galiotis, Nat. Commun. **2**, 255 (2011).

[20] O. Frank, M. Mohr, J. Maultzsch, C. Thomsen, I. Riaz, R. Jalil, K. S. Novoselov, G. Tsoukleri, J. Parthenios, K. Papagelis, L. Kavan, and C. Galiotis, ACS Nano **5**, 2231 (2011).

[21] J.-U. Lee, D. Yoon, and H. Cheong, Nano Lett. **12**, 4444 (2012).

[22] C. W. Huang, R. J. Shiue, H. C. Chui, W. H. Wang, J. K. Wang, Y. Tzeng, and C. Y. Liu, Nanoscale **5**, 9626 (2013).

[23] D. Yoon, Y. W. Son, and H. Cheong, Phys. Rev. Lett. **106**, 155502 (2011).

[24] M. Huang, H. Yan, T. F. Heinz, and J. Hone, Nano Lett. **10**, 4074 (2010).

[25] V. N. Popov and P. Lambin, Carbon **54**, 86 (2013).

[26] C. Thomsen, S. Reich, and P. Ordejón, Phys. Rev. B **65**, 073403 (2002).

[27] M. Mohr, J. Maultzsch, and C. Thomsen, Phys. Rev. B **82**, 201409(R) (2010).

[28] A. H. Castro Neto and F. Guinea, Phys. Rev. B **75**, 045404 (2007).

[29] K.-i. Sasaki, K. Kato, Y. Tokura, S. Suzuki, and T. Sogawa, Phys. Rev. B **86**, 201403 (2012).

[30] J. Yan, Y. Zhang, P. Kim, and A. Pinczuk, Phys. Rev. Lett. **98**, 166802 (2007).

[31] T. Ando, J. Phys. Soc. Jpn. **75**, 124701 (2006).

[32] M. Lazzeri and F. Mauri, Phys. Rev. Lett. **97**, 266407 (2006).

[33] S. Pisana, M. Lazzeri, C. Casiraghi, K. S. Novoselov, A. K. Geim, A. C. Ferrari, and F. Mauri, Nat. Mater. **6**, 198 (2007).

[34] V. M. Pereira, A. H. Castro Neto, and N. M. R. Peres, Phys. Rev. B **80**, 045401 (2009).

[35] M. O. Goerbig, J.-N. Fuchs, G. Montambaux, and F. Piéchon, Phys. Rev. B **78**, 045415 (2008).

[36] S. Katayama, A. Kobayashi, and Y. Suzumura, J. Phys. Soc. Jpn. **75**, 054705 (2006).

[37] A. Kobayashi, S. Katayama, Y. Suzumura, and H. Fukuyama, J. Phys. Soc. Jpn. **76**, 034711 (2007).

[38] T. Morinari, T. Himura, and T. Tohyama, J. Phys. Soc. Jpn. **78**, 023704 (2009).

[39] M. Assili and S. Haddad, J. Phys.: Condens. Matter **25**, 365503 (2013).

[40] K.-i. Sasaki, R. Saito, G. Dresselhaus, M. S. Dresselhaus, H. Farhat, and J. Kong, Phys. Rev. B **77**, 245441 (2008).

[41] D. P. DiVincenzo and E. J. Mele, Phys. Rev. B **29**, 1685 (1984).

[42] T. Ando, J. Phys. Soc. Jpn. **74**, 777 (2005).

[43] P. Marconcini and M. Macucci, Riv. Nuovo Cimento **34**, 489 (2011).

[44] G. Montambaux, F. Piéchon, J.-N. Fuchs, and M. O. Goerbig, Phys. Rev. B **80**, 153412 (2009).

[45] H. Suzuura and T. Ando, Phys. Rev. B **65**, 235412 (2002); J. Phys. Soc. Jpn. **77**, 044703 (2008).

[46] K. Ishikawa and T. Ando, J. Phys. Soc. Jpn. **75**, 084713 (2006).

[47] J.-N. Fuchs, arXiv:1306.0380.

[48] Y. Suzumura, T. Morinari, and F. Piéchon, J. Phys. Soc. Jpn. **82**, 023708 (2013).

[49] M. Monteverde, M. O. Goerbig, P. Auban-Senzier, F. Navarin, H. Henck, C. R. Pasquier, C. Mézière, and P. Batail, Phys. Rev. B **87**, 245110 (2013).

[50] K.-i. Sasaki, K. Wakabayashi, and T. Enoki, Phys. Rev. B **82**, 205407 (2010).

[51] M. Assili and S. Haddad (unpublished).